IN-CYLINDER OH AND CO₂* DETECTION IN SI ENGINE THROUGH UV NATURAL EMISSION SPECTROSCOPY

Simona Silvia Merola¹⁾, Cinzia Tornatore²⁾, Luca Marchitto³⁾, Gerardo Valentino⁴⁾

Istituto Motori, National Research Council of Italy
Viale G. Marconi, 4, 80125 Naples, Italy
tel.: +39 081 7177224¹⁾, +39 081 7177103²⁾
+39 081 7177119³⁾, +39 081 7177129³⁾
e-mail: s.merola@im.cnr.it¹⁾, c.tornatore@im.cnr.it²⁾
l.marchitto@im.cnr.ii³⁾t, g.valentino@im.cnr.it⁴⁾

Abstract

Processes of the combustion of liquid fuels and solid are more complex than combustion of fuel gases. With reference to liquid fuels occur additionally processes of vaporization of the fuel, and with reference to solid fuels – decomposition of the solid phase with processes of melting and vaporization, pyrolysis, or gasification. This simultaneous and also different influence of different parameters is sometimes a reason of incorrect interpretation of experimental results. The study of the theoretical model of the combustion process concerning of liquid and solid fuels and which then the model takes into account also the gas- phase, because combustion processes take place in this phase, and occurs the interaction of the phase gas- and liquid or the solid one. The theoretical model is presented basing on experimental initial researches realized in a model with reference to liquid fuels and solid ones. Researches realized in the constant volume chamber with measurements of the pressure during the process of the combustion with the use of quick photography and with measurement of the distribution of the velocity in the spray of the fuel and droplet measurements by means the laser Doppler equipment LDV and PDPA. There were obtained a good agreement of findings experimental researches with the theoretical model. Generally, on the combustion velocity of liquid fuels and solid one significant influence has a kind (laminar, temporary and turbulent) and the thickness of the thermal boundary layer.

Keywords: road transport, simulation, combustion engines, air pollution, environmental protection

1. Introduction

Light duty spark ignition engines are forecasted to remain the dominant benchmark in the passenger car market segment for the foreseeable future [1]. Currently the driver for innovations concerning the powertrain itself is mainly the reduction of fuel consumption, which is directly connected to meeting CO₂ emissions limits. This results in diverse solutions depending on the vehicle market and the engine class. Next to measures concerning a robust combustion concept design for extreme downsized engines, alternative transmission concepts and several hybrid vehicle architectures variants are also discussed. Boosting systems are a key technology enabler for gasoline engine downsizing to ensure acceptable performance whilst increasing efficiency. In spite of the strong improvement realised in the next years, further steps are needed for boosted engines optimisation [2]. To reach this target, a better understanding of the thermo-fluid dynamic phenomena occurring during the combustion process is required. To this aim, this paper reports the results obtained by experimental investigations of the combustion process and pollutant formation in a port fuel injection (PFI) SI boosted engine. High spatial and temporal resolution optical techniques were applied in the combustion chamber of a partially transparent engine. Cycle-resolved visualization was applied to follow the flame propagation from the spark ignition to the exhaust phase. UV natural emission spectroscopy allowed the detection of the chemical markers of the combustion process with specific interest for OH radicals and CO₂*.

2. Experimental apparatus

The engine used for the experiments was an optically accessible single cylinder PFI SI engine. It was equipped with the cylinder head of a commercial SI turbocharged engine with the same geometrical specifications. Further details on the engine are reported in Tab. 1. The head had four valves and a centrally located spark plug. The injection system was a commercial one 10-hole injector. An external air compressor was used to simulate boosted conditions of intake air pressure and temperature in a range of 1000 - 2000 mbar and 290 – 340 K, respectively.

A quartz pressure transducer was flush-installed in the region between intake-exhaust valves at the side of the spark plug. The transducer allowed to perform in-cylinder pressure measurements in real-time. An elongated engine piston was used, it was flat and its upper part was transparent since it was made of fused silica UV enhanced (Φ=57mm). To avoid the window contamination by lubricating oil, self-lubricant Teflon-Bronze composite piston rings were used in the optical section. To reduce the initial conditions effects, the engine was preheated by a conditioning unit, and it was maintained in motored condition by an electrical engine until the temperature reached 65°C. After the warm-up, the engine worked in fired conditions for 300 consecutive cycles. The engine parameters and pressure measured in the last 200 cycles were considered in the work. Then the engine returned in motored condition for 100 cycles. This phase allowed checking a possible change in thermal and fluid-dynamic status of the engine from the beginning of the measurements. National Instruments LabVIEW acquisition-system driven by an optical encoder with 0.1 crank angle degree resolution recorded the TTL signals from the high-speed camera acquisitions and the pressure transducer. In this way, it was possible to determine the crank angles at which the optical measurements were carried out.

Displaced volume	399 cc	
Stroke	81.3 mm	
Bore	79 mm	
Connecting Rod	143 mm	
Compression ratio	10:1	
Number of Valves	4	
Exhaust Valve Open	153 CAD ATDC	
Exhaust Valve Close	360 CAD ATDC	
Inlet Valve Open	357 CAD ATDC	
Inlet Valve Close	144 CAD BTDC	

Tab. 1. Specifications of the single cylinder optical engine

Figure 1 shows the experimental apparatus for the optical investigations and the bottom field of view of the combustion chamber. During the combustion process, the light passed through a quartz window located in the piston and it was reflected toward the optical detection assembly by a 45° inclined UV-visible mirror located at the bottom of the engine.

Cycle resolved flame visualization was performed using an Optronis mod. CamRecord 5000 high-speed camera. It was a CMOS monochrome image sensor, its full chip dimension was 512x512 pixels and the pixel size was 16x16 µm. The camera A/D Conversion was 8 bit and the spectral range extended from 390 nm to 900 nm. The camera was equipped with a 50 mm focal Nikon lens, a camera region of interest was selected (400 x 400 pixel) to obtain the best match between spatial and temporal resolution. All the images are a line-of-sight average. The exposure time was fixed at 25 µs and the frame rate was 6470 fps. In this work, the optical measurements were performed during 100 consecutive engine cycles after an engine warm-up under motored conditions and 100-fired cycles.

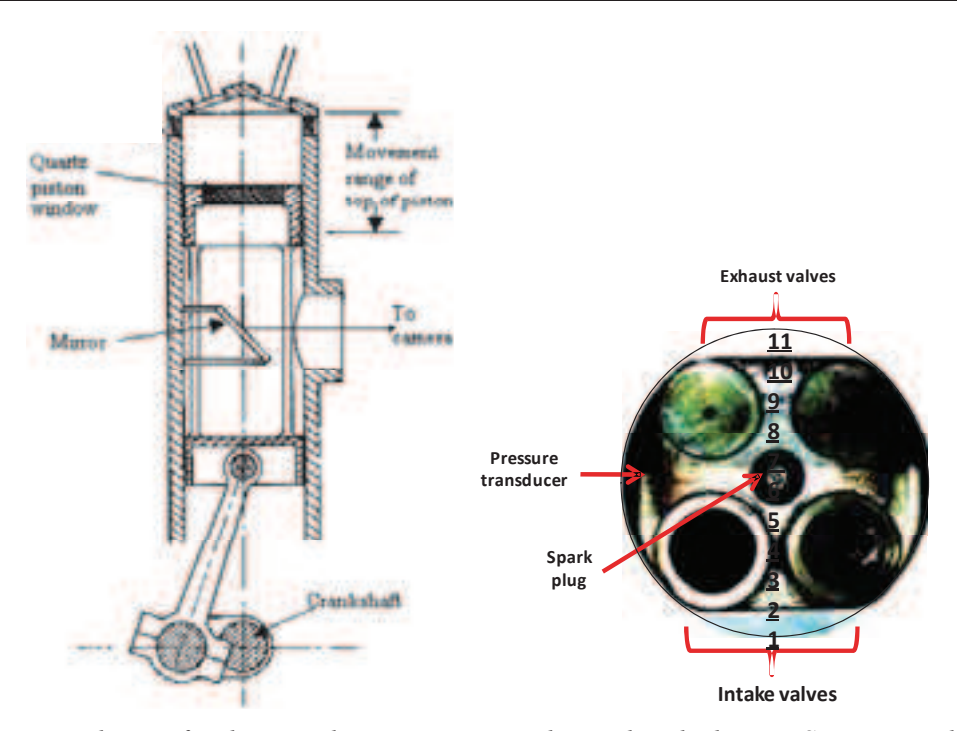


Fig. 1. Experimental setup for the optical measurements in the single cylinder PFI SI engine with the bottom field of view of the combustion chamber

For spectroscopic investigations, the radiative emissions from the combustion chamber were focused by a 78 mm focal length, f/3.8 UV Nikon objective onto the micrometer controlled entrance slit of a spectrometer with 150 mm focal length and 600 groove/mm grating (central wavelength 350 nm) From the grating the radiations were detected by an intensified CCD camera (array size of 1024 x 1024 pixels with a pixel size of 13x13 µm and 16-bit dynamic range digitization at 100 kHz). The exposure time was fixed at 41.6 µs and the dwell time between two consecutive acquisitions was set at 60 µs. Spectroscopic investigations were carried out in the central region of the combustion chamber. Region of interest for spectroscopic investigation included 512 rows (or spectra) and it was divided in 8 locations. To enhance signal to noise ratio the 64 spectra of each location were averaged. The spectra were corrected for the optical setup efficiency using a deuterium lamp with a highly uniform full spectrum. The wavelength calibration was performed using a mercury lamp.

The time evolution of combustion products was evaluated from spectroscopic investigations using a post-processing procedure. For each chemical species with well-resolvable narrow emission bands, the height of the band expressed in counts was evaluated after the subtraction of emission background and other species contribution. Thus, OH emission was evaluated as height of the 310 nm band system after the subtraction of the emission background, evaluated as the mean value between the emissions measured at 300 nm and 320 nm. For broadband emission, the mean intensity, at specific wavelength range, was considered. Thus, CO_2 * emission was evaluated as mean intensity at 350-360 nm. A routine, developed in Labview environment, allowed to simultaneously evaluating the emissions of the selected compounds and species for each spectrum and each time. Moreover, OH and CO_2 * emissions were calculated as average on all the spectra.

3. Results

Tested operative conditions are listed in Tab. 2. In particular, the injection timings were fixed in order to inject the fuel when the intake valves were closed (CV) and open (OV), respectively. The duration of injection (DOI) was changed for setting $\lambda = 1.0 \ (\pm 3\%)$ as measured by a lambda sensor at the engine exhaust and averaged over 200 consecutive engine cycles. For the selected

spark timing, the IMEP was the comparable in both the injection conditions; related variation (COV) was lower than 3%.

In PFI engine, the fuel is generally injected at the backside of a closed intake valve to take advantage of the warm valve and port surfaces for vaporization [3-5]. However, a large part of the injected spray is deposited on the intake manifold surfaces and forms a layer of liquid film on the valve and port surfaces. The film needs to be re-atomized by the shearing airflow as the intake valves open. If these fuel layers are not well atomized they enter the cylinder as drops and ligaments [6-8]. These phenomena occur in varying degrees and depend upon the engine design, injector location and engine operation.

Tab. 2. Operative conditions

Engine speed	2000 rpm		
Abs intake air pressure	1.4 bar		
Abs. intake air temperature	338 K		
Relative injection pressure	3.5 bar		
Throttle position	Wide open		
Exhaust Valve Open	153 CAD ATDC		
Exhaust Valve Close	360 CAD ATDC		
Inlet Valve Open	357 CAD ATDC		
Inlet Valve Close	144 CAD BTDC		
Spark timing	18 CAD BTDC		
Test label	OV	CV	
Injection timing	300 CAD BTDC	130 CAD ATDC	
Duration of injection	148 CAD	155 CAD	
IMEP	12.3 bar 12.4 bar		
COV	1.9	2.4	

Previous experiments on the same engine fuelled by gasoline demonstrated that the injector sprayed the fuel towards the plate between the intake valves and on the intake valves stems [9, 10]. The droplets impingement induced fuel layer formation on the intake manifold walls. The fuel layers were drawn by gravity on the valve head and gap, where they remained as film due to the surface tension. The stripping of the squeezed fuel film created fuel deposits on the optical window. When the injection occurred in open valve condition, part of the droplets was carried directly into the combustion chamber by the gas flow. These droplets, sucked in the combustion chamber, stuck on the cylinder walls. In both injection conditions, the fuel deposits on the combustion chamber walls created fuel-rich zones on the piston surfaces that influenced the composition of the mixture charge and hence the combustion process. Cycle resolved imaging of the combustion process was performed using the high-speed camera. Fig. 2 and 3 reports the flame propagation detected in the combustion chamber for the closed valve and open valve injection conditions. In good agreement with the results reported in previous works [11] the flame front started from the centrally located spark plug and it spread with radial-like behaviour for around 15 CAD after the spark (AS). After this time, the flame front shape showed an asymmetry: the flame reached first the cylinder walls in the exhaust valves region. This was due to the fuel film deposited on the intake valves. Several bright spots were detected in the burned gas before the flame front reached the chamber walls. These bright spots were due to the fuel deposits on the quartz window. The fuel deposits locally created fuel-rich zones with millimetre size that ignited when reached by the normal flame front. Clear evidence of bright spots can be noted in the open valves condition. This was caused by the carrying of the injected fuel droplets directly into the combustion chamber by the gas flow. A proportion of these droplets stuck on the cylinder walls and a part was deposited on the piston surface.

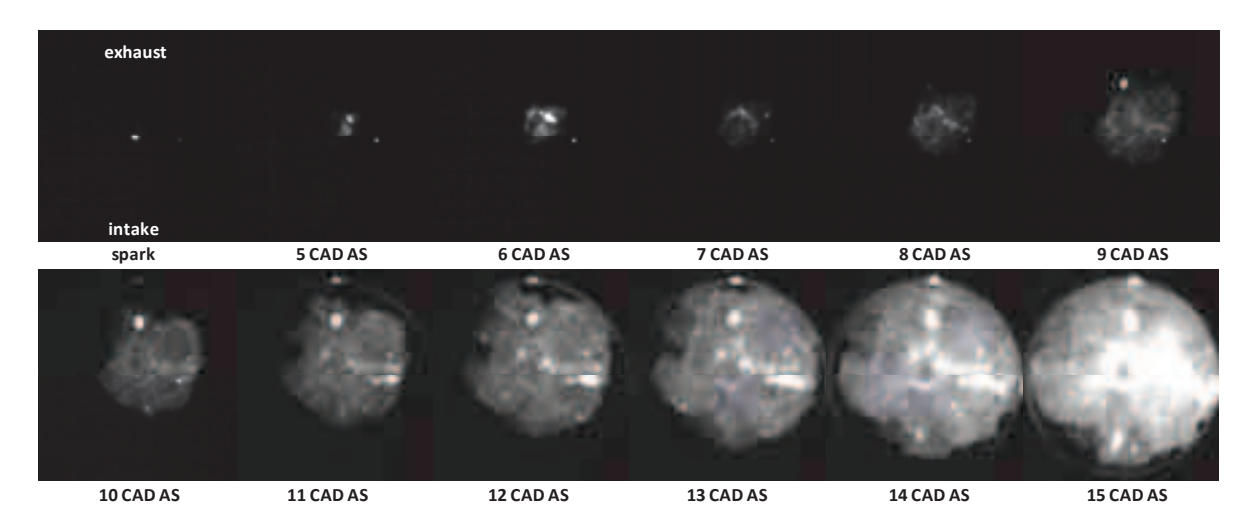


Fig. 2. Cycle-resolved flame propagation detected for the closed valve injection condition (CV)

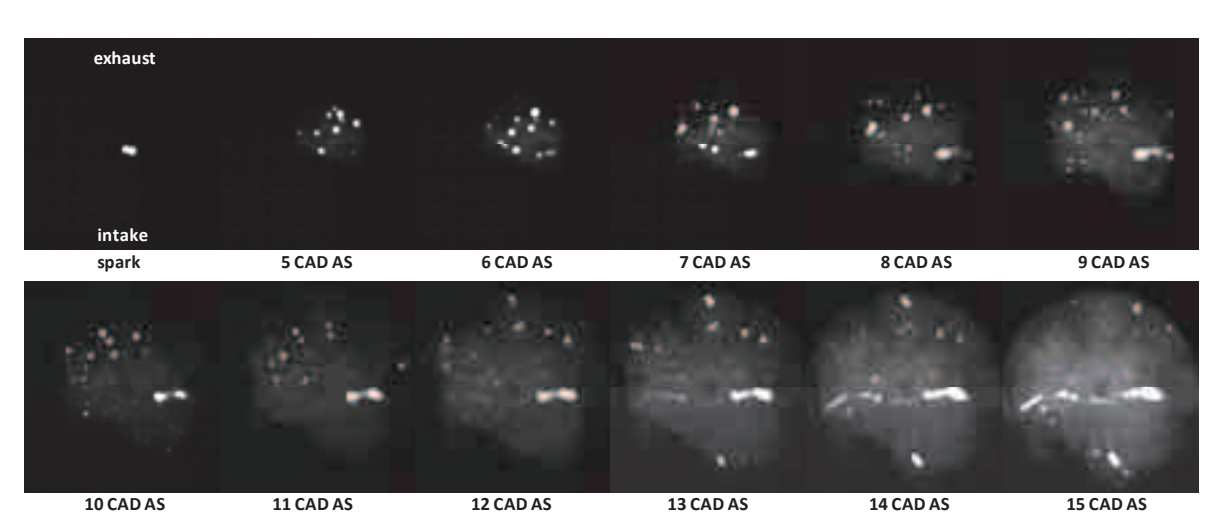


Fig. 3. Cycle-resolved flame propagation detected for the open valve injection condition (OV)

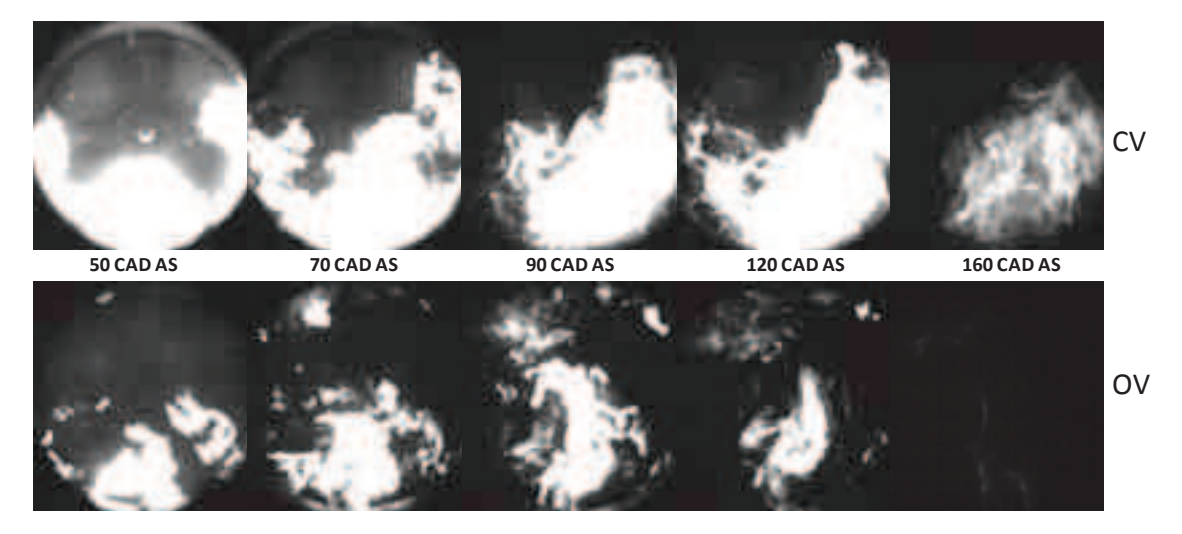


Fig. 4. Cycle-resolved flame emission detected in the last combustion phase

Figure 4 reports the last phase of the combustion process detected for both operating conditions. The selected images show an abnormal combustion that takes place when the flame front reaches the intake valves. The effect occurs because of the interaction between the flame front and the fuel film deposits on the intake-valves. In fact it is possible to achieve gas temperature and mixture strength conditions that lead to fuel film ignition, creating a diffusion-controlled flame that can persist well after the normal combustion event. In the closed valve condition, an intense diffusion-controlled flame was observed especially near the intake valves and it was present until the opening of the exhaust valves. In the open-valve condition the flame near the intake valves was less intense due to the lower amount of deposited fuel. Moreover, a diffusive flame could be detected also in the exhaust valves region. It was caused by the burning of the fuel film formed on the combustion chamber walls during the injection in open-valve condition. [9, 12].

In order to identify the chemical species that featured the combustion process from the spark ignition until the exhaust valve opening, natural emission spectroscopy was applied. Fig. 5 shows the typical spectrum detected at the spark ignition in the location 5 and 6 for the CV condition.

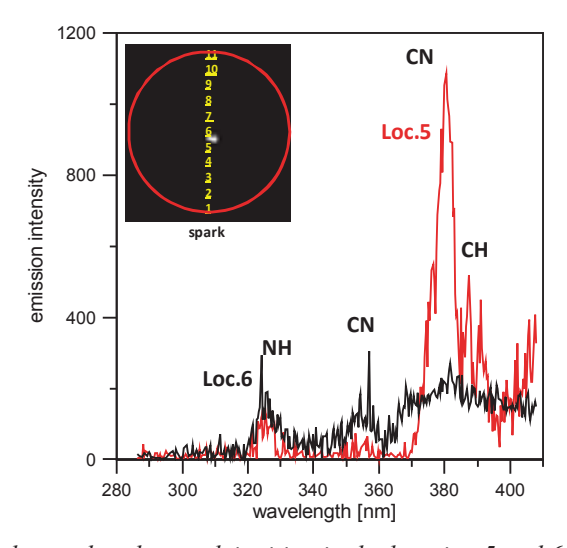


Fig. 5. UV spectrum detected at the spark ignition in the location 5 and 6 for the OV condition

The most identifiable features of the plasma emission are labelled with the corresponding chemical species. The interaction between the excited hydrocarbon species and the surrounding air molecules was detected by the presence of CN and NH [13, 14]. The CN violet band system is featured by two bands at 388.3 nm (the strongest band) and at 359.0 nm. The band at 421 nm is only partially evident at the limit of the selected spectral range. NH is detected through the emission band at 336 nm due to ${}^{3}\Pi$ - ${}^{3}\Sigma$ transition. Regarding CH system at 390 nm and 314 nm: the first, due to the transitions ${}^{2}\Sigma$ - ${}^{2}\Pi$, is detectable close to CN band. It strongly degraded towards the red and overlapped to the tail of CN emission at 421 nm. The 314 nm band is very weak and hidden by NH emission.

Figure 6 shows typical natural emission spectra detected in the combustion chamber during the flame front propagation. At 8 CAD after spark, the flame front already showed the asymmetrical shape due to the fuel deposition on the intake valves. The UV spectra are featured by the strong emission band of OH (310 nm) due to the A-X diagonal transitions [15]. The radical emission decreases from the burned gas towards the reaction zone due to the temperature gradient. This occurs because OH radicals are intermediate and very active compounds generated during the combustion process in the reaction zone by the dissociation of H₂O₂ at high temperatures. All the spectra, expect that one detected in location 5 that corresponds to the reaction zone, are also characterized by a background signal, which is essentially constant with wavelength between 280 and 400 nm. It is primarily due to CO₂* emission [13]. It is known that CO₂* alone accounts to more than 90% of the signal integrated over the entire flame spectrum. It should be noted that a higher concentration of OH radicals reduces the emissions of CO since they help to complete the oxidation from CO to CO₂ [16].

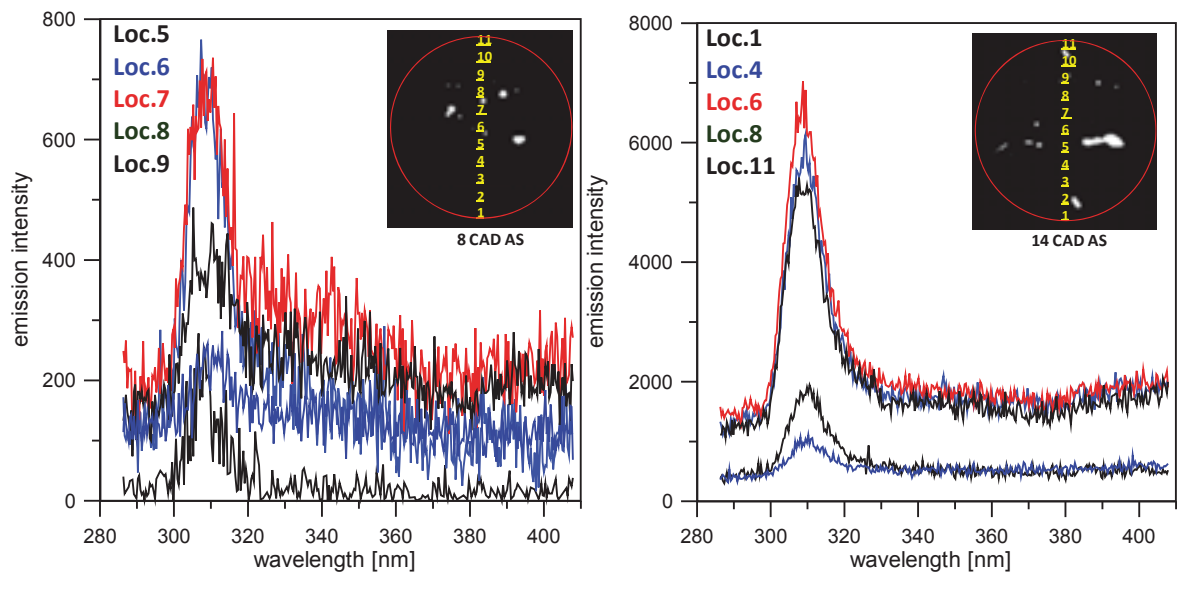


Fig. 6. Natural emission spectra detected in selected locations of the combustion chamber at 8 and 14 CAD after spark (AS) in OV condition

OH is also involved in the formation of NO, since it is the only indicator of the formation of NO by the Zeldovich mechanism [17]. At 14 CAD AS the flame front reached the valves region; the spectral behaviours measured in the different location resulted similar and only an emission intensity increase was detected. Only in the late combustion phase different spectral behaviour were observed in the different combustion chamber locations. As shown in Fig. 7, the diffusion-controlled flames around the intake valves induced a strong continuous contribution to the emission that increased with the wavelength in the visible range (Loc. 2). This trend was typical of blackbody-like emission of the soot particles. The luminous intensity was related to different soot concentration. The evidence in the late combustion phase of OH is due to the role of the radical in the soot oxidation [18, 19]. It should be noted that the late combustion spectra were featured by a band around 325 nm due to OH off-diagonal A-X transition [13]. Similar results were obtained by spectroscopic investigation of combustion process for closed-valve injection condition.

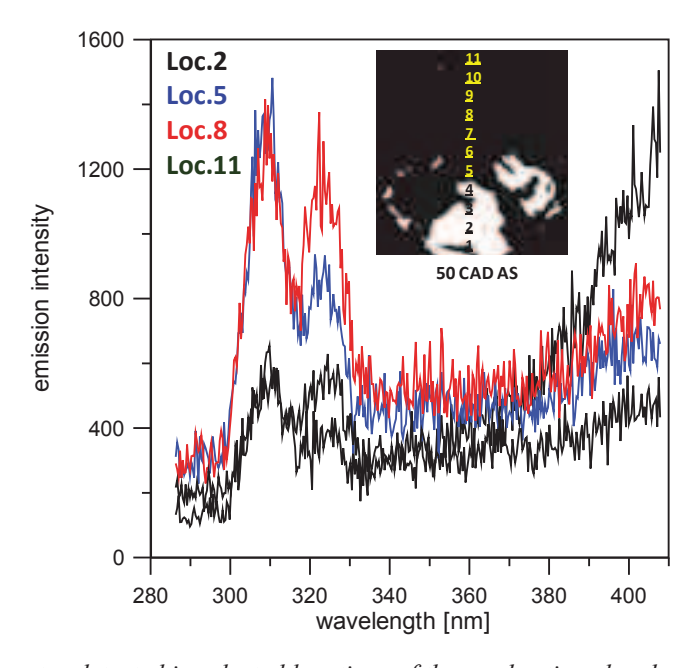


Fig. 7. Natural emission spectra detected in selected locations of the combustion chamber at 50 CAD after spark (AS) in OV condition

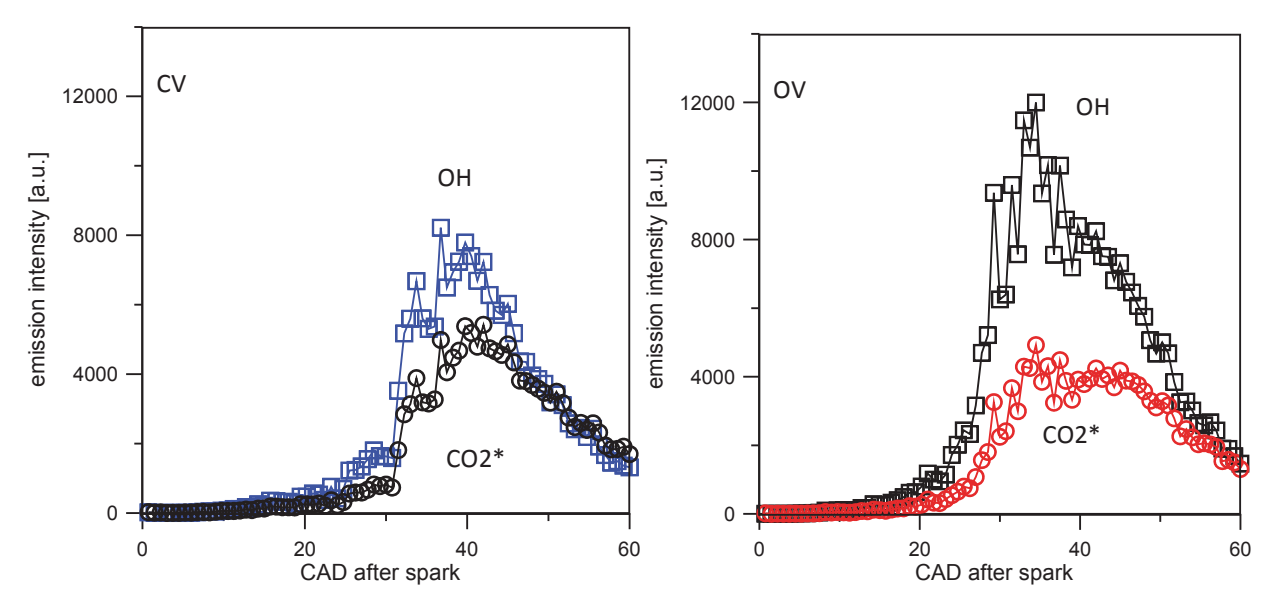


Fig. 8. Time evolution of OH and CO2*as evaluated from spectroscopic data for CV (left) and OV (right) fuel injection condition

Using the retrieving procedure previously described, time evolution of OH and CO₂* were evaluated for both the engine operating conditions. The results are reported in Fig. 8. OH reached the maximum value around 30-35 CAD after the spark for both the conditions. The higher emission for OV case is in agreement with higher NOx emission measured at the exhaust and reported in Tab. 3. On the other hand CO₂* showed comparable trend with highest intensity around 40 CAD after spark. After this time the CO₂ molecules should very slowly decrease until the exhaust. On the other hand, the diagnostics used in this work was able to follow the evolution of CO₂ only in the excitation state, thus a faster reduction was measured. Anyway, the CO₂* highest value can be correlated to CO₂ exhaust in good agreement.

	CO %	CO ₂ %	HC ppm	NOx ppm
CV	0.38	12.8	566	2835
OV	0.5	12.3	561	3177

Tab. 3. Exhaust gas emissions

Conclusions

Cycle resolved digital imaging and UV natural emission spectroscopy were applied in a single cylinder optically accessible spark ignition engine to investigate the combustion process and pollutant formation. Digital imaging allowed following the flame front propagation from the spark timing until the opening of the exhaust valve. Abnormal combustion effects due to the burning of fuel film deposition on the intake valves and piston surfaces were put in evidence together to the normal combustion evolution. Spectroscopic investigations permitted the simultaneous detection and consequent spatial and time evolution analysis of OH radicals and CO₂*. OH radicals were linked to nitrogen oxide emission and to the oxidation of soot precursors formed by fuel deposition burning. CO₂* was correlated to CO₂ exhaust. Finally, the detection of CO₂ molecules in the excitation state allowed distinguishing the contribution of the combustion process to carbon oxides formation from that due to other mechanism such as the EGR.

References

- [1] Berggren, C., Magnusson, T., Reducing automotive emissions The potentials of combustion engine technologies and the power of policy Original Research Article, Energy Policy, Vol. 41, pp. 636-643, 2012.
- [2] Heywood, J. B., Kasseris, E., Comparative Analysis of Automotive Powertrain Choices for the Next 25 Years, SAE Paper No. 2007-01-1605, 2007.
- [3] Henein, N. A., Tagomori, M. K., *Cold-start hydrocarbon emissions in port-injected gasoline engines*, Progress in Energy and Combustion Science, 25, pp. 563–593, 1999.
- [4] Behnia, M., Milton, B. E., Fundamentals of fuel film formation and motion in SI engine induction systems, Energy Conversion and Management, 42(15-17), pp. 1751-1768, 2001.
- [5] Costanzo, V. S., Heywood, J. B., *Mixture Preparation Mechanisms in a Port Fuel Injected Engine*, SAE Technical Paper n. 2005-01-2080, 2005.
- [6] Gold, M. R., Arcoumanis, C., Whitelaw, J. H., Gaade, J., Wallace, S., *Mixture Preparation Strategies in an Optical Four-Valve Port-Injected Gasoline Engine*, Int. J. of Engine Research, 1(1), pp. 41-56, 2000.
- [7] Nogi, T., Ohyama, Y., Yamauchi, T., Kuroiwa, H., *Mixture Formation of Fuel Injection Systems in Gasoline Engines*, SAE Technical Paper n. 880558, 1988.
- [8] Meyer, R., Heywood, J. B., Liquid Fuel Transport Mechanisms into the Cylinder of a Firing Port-Injected SI Engine During Start Up, SAE Technical Paper n. 970865, 1997.
- [9] Merola, S. S., Vaglieco, B. M., Optical investigations of fuel deposition burning in ported fuel injection (PFI) spark-ignition (SI) engine, Energy, 34, pp. 2108–2115, 2008.
- [10] Merola, S. S, Sementa, P., Tornatore, C., Vaglieco, B. M., *Effect of Injection Phasing on Valves and Chamber Fuel Deposition Burning in a PFI Boosted Spark-Ignition Engine*, SAE International Journal of Fuels and Lubricants Vol. 1 No. 1 pp. 192-200, 2009.
- [11] Merola, S. S., Sementa, P., Tornatore, C., Vaglieco, B. M., *Effect of the fuel injection strategy on the combustion process in a PFI boosted spark-ignition engine*, Energy, Vol. 35, Is. 2, pp. 1094-1100, 2010.
- [12] Witze, P. O., Green, R. M., LIF and Flame-Emission Imaging of Liquid Fuel Films and Pool Fires in an SI Engine During a Simulated Cold Start, SAE Paper No. 970866, 1997.
- [13] Gaydon, A. G., The Spectroscopy of Flames, Chapman and Hall ltd., 1957.
- [14] Alkemade, C. Th. J., Herrmann, R., Fundamentals of Analytical Flame Spectroscopy, Hilger, Bristol, UK 1979.
- [15] Dieke, G. H., Crosswhite, H. M., *The ultraviolet bands of OH.* J. Quant. Spectrosc. Radiat. Transfer, 2, 97-199, 1962.
- [16] Bowman, C. T., *Kinetics of pollutant formation and destruction in combustion*, Progress in Energy and Combustion Science, Vol. 1, No. 1, pp. 33-45, 1975
- [17] Miller, J. A., Bowman, C. T., *Mechanism and modeling of nitrogen chemistry in combustion*, Progress in Energy and Combustion Science, Vol. 15, Is. 4, pp. 287-338, 1989.
- [18] Fenimore, C. P., Jones, G. W., Oxidation of soot by hydroxyl radicals, J. Phys. Chem., 71 (3), pp. 593–597, 1967
- [19] Puri, R., Santoro, R. J., Smyth, K. C., *The oxidation of soot and carbon monoxide in hydrocarbon diffusion flames*, Combustion and Flame, Vol. 97, Is. 2, pp. 125-144, 1994.